Concentration effect of the near-infrared quantum cutting of 1788-nm luminescence of Tm^{3+} ion in $(Y_{1-x}Tm_x)_3Al_5O_{12}$ powder phosphor*

Chen Xiao-Bo(陈晓波)[a)†], Li Song(李 崧)[a)], Ding Xian-Lin(丁贤林)[b)], Yang Xiao-Dong(杨小冬)[a)], Liu Quan-Lin(刘泉林)[b)], Gao Yan(高 燕)[c)], Sun Ping(孙 萍)[a)], and Yang Guo-Jian(杨国建)[a)]

[a)] *Department of Physics and Applied Optics Beijing Area Major Laboratory, Beijing Normal University, Beijing* 100875, *China*
[b)] *School of Materials Science and Engineering & State Key Laboratory for Advanced Metals and Materials, University of Science and Technology of Beijing, Beijing* 100083, *China*
[c)] *Laboratory of Nanomaterials, National Center for Nanoscience and Technology of China, Beijing* 100190, *China*

(Received 28 February 2014; revised manuscript received 27 April 2014; published online 10 June 2014)

In the present paper, the concentration effect of near-infrared quantum cutting of Tm^{3+} ion in $(Y_{1-x}Tm_x)_3Al_5O_{12}$ powder phosphor is studied by means of experiments and calculations. In addition, the absorption spectra, visible-to-near-infrared excitation and emission spectra, and fluorescence lifetimes are measured. It is found that $(Y_{1-x}Tm_x)_3Al_5O_{12}$ powder phosphor has a strong four-photon near-infrared quantum cutting luminescence of 1788.0-nm $^3F_4 \rightarrow {}^3H_6$ fluorescence of Tm^{3+} ion, when excited by 357.0-nm light. It is also found that the up-limit of the four-photon near-infrared quantum cutting luminescence efficiency of $(Y_{0.700}Tm_{0.300})_3Al_5O_{12}$ powder phosphor is approximately 302.19%. To the knowledge of the authors, this is the first time that a near-infrared quantum cutting efficiency up-limit exceeding 300% has been reported. The results of this manuscript are valuable in aiding the probing of the new generation Ge solar cell.

Keywords: near-infrared quantum cutting, luminescence, $(Y_{1-x}Tm_x)_3Al_5O_{12}$ powder phosphor, energy transfer, germanium solar cell

PACS: 78.55.–m, 78.56.–a, 78.30.–j **DOI:** 10.1088/1674-1056/23/8/087809

1. Introduction

Searching for new sources of energy has become one of the most important projects of research throughout the world, and the most ideal new energy source is currently solar energy.[1–8] Solar energy is very abundant, and the energy irradiated onto the Earth for 50 minutes can meet the energy consumption needs of the entire world for an entire year. Solar energy is also inexhaustible. At the same time, solar electric power is also a very clean source of energy as it creates no pollution whatsoever, thus solar electric power is praised as currently the most ideal source of energy. However, there is a great disparity between the utilization and reserve of solar energy, due to the fact that solar cells have high cost and low efficiency[2,3] as 70% of all energy losses are related to transmission loss and thermalization loss. Therefore a prospective method to enhance solar cell efficiency by quantum cutting is the cutting of a high-energy photon into multiple low-energy photons to adapt the solar spectrum, thus more effectively matching the solar cell.[1–13]

At present, new theories, materials, techniques, designs, and products related to solar cells have been developed at a very rapid speed.[1–19] The development of germanium (Ge) solar cells as a new type of solar cells with a narrow band-gap width is very interesting, and has been used in germanium, silicon–germanium, and cascade three-junction solar cells.[4,13,17] The germanium solar cell has the characteristic advantages of a small band-gap width of 0.67 eV: 300 K (5404 cm^{-1} = 1850.5 nm).[1–8] And it can absorb almost all near-infrared solar spectra quite effectively. Therefore, its transmission loss is very small and almost negligible.[15] If the solar spectra from ultraviolet to visible region can be converted into near-infrared region at about 1800 nm by means of quantum cutting, then the absorption efficiency of the Ge solar cell will be greatly enhanced. Furthermore, the radiative photon numbers can be very greatly enhanced by multiphoton quantum cutting, so can the electron–hole pair numbers of the Ge solar cell. It is also very possible that the opto-electricity conversion efficiency of the Ge solar cell will be very greatly enhanced, as it may have great acceleration effects on solar cell project research.[20]

Ever since the second-order near-infrared quantum cutting in $Yb_xY_{1-x}PO_4$:Tb^{3+}, used for the development of Si solar cells, was first reported by Vergeer and Meijerink in 2005,[2] the importance, application, and significance of the near-infrared quantum cutting phenomenon have been widely recognized.[1–25] Quantum cutting also is one of the impor-

*Project supported by the National Natural Science Foundation of China (Grant No. 10674019) and the Significant Project of Fundamental Research Funds for the Central Universities of China (Grant No. 212-105560GK).

†Corresponding author. E-mail: chen78xb@sina.com

© 2014 Chinese Physical Society and IOP Publishing Ltd

tant applications of rare earth.[21,25] Since 2007, near-infrared quantum cutting has become an international hot research topic. And about 80 relevant papers have been published in a range of top journals.[2,5–12,26–30] However, regarding near-infrared quantum cutting of about 1800-nm luminescence of Tm^{3+} ion activator center, only six papers have been reported up to now.[5,8,10,14,27] The present paper studies the concentration effect of the near-infrared multiphoton quantum cutting luminescence phenomena of $(Y_{1-x}Tm_x)_3Al_5O_{12}$ powder phosphor. It is found for the first time that the up-limit of the four-photon near-infrared quantum cutting luminescence efficiency of $(Y_{0.7}Tm_{0.3})_3Al_5O_{12}$ powder phosphor is approximately 302.19%. To the knowledge of the authors, this is the first time that a near-infrared quantum cutting efficiency up-limit exceeding 300% has been reported.

2. Experimental samples and experimental devices

The samples used in our experiment were (A) $(Y_{0.9975}Tm_{0.0025})_3Al_5O_{12}$, (B) $(Y_{0.995}Tm_{0.005})_3Al_5O_{12}$, (C) $(Y_{0.900}Tm_{0.100})_3Al_5O_{12}$, (D) $(Y_{0.800}Tm_{0.200})_3Al_5O_{12}$, and (E) $(Y_{0.700}Tm_{0.300})_3Al_5O_{12}$ powder phosphors. The Tm:YAG powder samples were prepared through a solid-state reaction. The starting materials were high-purity Y_2O_3 (99.99%), Al_2O_3 (99.99%), and Tm_2O_3 (99.99%). The raw powders were weighted according to the stoichiometric compositions, and then it was sequentially mixed, ground, and pressed into pellets. Finally, the powders were sintered at 1600 °C for 2 h in a furnace in air.

The experimental equipment used was the Fluorescence Spectrometer FL3-2iHR, produced by the Horiba-JY Company. The pumping light source was an Xe lamp. The visible detector used was an R2658p photomultiplier, which has a very high sensitivity in a range from 250 nm to 1000 nm. The infrared detector used was a solid state indium antimony detector DSS-IS020L, which has a high sensitivity in a range from 1000 nm to 5000 nm. For all of the experimental results, the experimental curves with the same wavelength in the same figure can be compared directly in terms of fluorescence intensity.

3. Absorption spectrum

Figure 1 shows the absorption spectrum of the $(Y_{0.700}Tm_{0.300})_3Al_5O_{12}$ powder phosphor, which is measured by a UV-3100 spectrophotometer (Shimadzu). It is found that there is a series of absorption peaks located at (1695.5, 1625.0), (1202.0, 1175.0), 782.0, 683.5, 465.0, and 359.5 nm respectively. It is easy to recognize that they are due to the absorption transitions of $^3F_4$, $^3H_5$, $^3H_4$, $^3F_3$, $^1G_4$, and $^1D_2$ energy levels of Tm^{3+} ion respectively.[7,18] From Fig. 1, it is also easy to see that the lowest Stark energy levels of $^3F_4$, $^3H_5$, $^3H_4$, $^3F_3$, $^3F_2$, $^1G_4$, and $^1D_2$ energy levels of Tm^{3+} ion are located at 1780.0, 1238.0, 804.0, 698.0, 662.0, 465.0, and 359.5 nm respectively. Moreover, it can be calculated from the above experimental data that the gravity center of $^3F_4$, $^3H_5$, $^3H_4$, $^3F_3$, $^3F_2$, $^1G_4$, and $^1D_2$ energy levels of Tm^{3+} ion are centered at 5911.9, 8342.5, 12790.6, 14517.7, 15105.7, 21505.5, and 27816.5 cm^{-1} wave-number respectively.

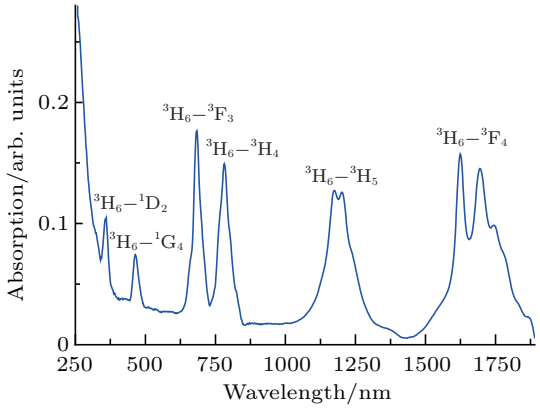


Fig. 1. (color online) The absorption spectrum of the $(Y_{0.700}Tm_{0.300})_3Al_5O_{12}$ powder phosphor.

4. Experimental excitation spectra

First, we measured the visible excitation spectra of (B) $(Y_{0.995}Tm_{0.005})_3Al_5O_{12}$, (C) $(Y_{0.900}Tm_{0.100})_3Al_5O_{12}$, and (E) $(Y_{0.700}Tm_{0.300})_3Al_5O_{12}$ powder phosphors in a wavelength range of 300 nm–710 nm, when the fluorescence received wavelength is 800.0 nm, and the results are shown in Fig. 2. It is found that the Tm:YAG powder phosphor has three groups of excitation spectrum signal peaks in a range from ultraviolet to visible, the main peaks of which are located at 357.0, 459.5, and 680.0 nm. It is easy to recognize that these are respectively due to the $^3H_6 \rightarrow {}^1D_2$, $^3H_6 \rightarrow {}^1G_4$, and $^3H_6 \rightarrow {}^3F_3$ absorption transitions of Tm^{3+} ion.[7,18] In the figure, the small 415.5-nm peak is noise, the small 658.0-nm peak is

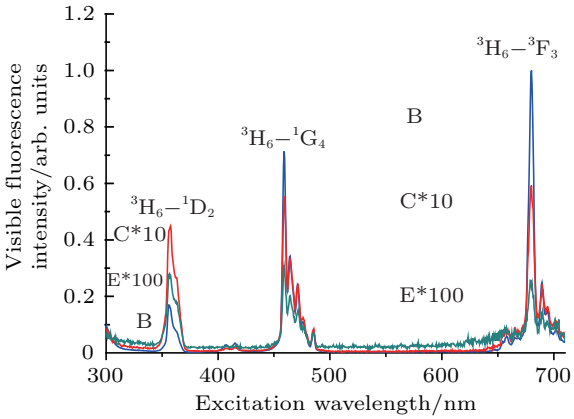


Fig. 2. (color online) Visible excitation spectra of (B) $(Y_{0.995}Tm_{0.005})_3Al_5O_{12}$ (blue), (C) $(Y_{0.900}Tm_{0.100})_3Al_5O_{12}$ (red), and (E) $(Y_{0.700}Tm_{0.300})_3Al_5O_{12}$ (green) powder phosphors, when the fluorescence received wavelength is located at 800 nm.

the $^3H_6 \rightarrow {}^3F_2$ absorption transitions of Tm^{3+} ion. B is the excitation spectrum signal of the (B) $(Y_{0.995}Tm_{0.005})_3Al_5O_{12}$ powder phosphor; C*10 is that of (C) $(Y_{0.900}Tm_{0.100})_3Al_5O_{12}$ powder phosphor, which is magnified 10 times; E*100 is that of (E) $(Y_{0.700}Tm_{0.300})_3Al_5O_{12}$, which is magnified 100 times.

Sequentially, we measured the excitation spectra of (B) $(Y_{0.995}Tm_{0.005})_3Al_5O_{12}$, (C) $(Y_{0.900}Tm_{0.100})_3Al_5O_{12}$, and (E) $(Y_{0.700}Tm_{0.300})_3Al_5O_{12}$ powder phosphor in a wavelength range of 300 nm–850 nm, when the fluorescence received wavelength is 1788.0-nm near-infrared wavelength, and the results are shown in Fig. 3. It is found that the Tm:YAG powder phosphor has four groups of excitation spectrum signal peaks from 300 nm to 850 nm, the main peaks of which are located at 357.0, 461.0, 680.0, and 780.0 nm. It is easy to recognize that they are respectively due to the $^3H_6 \rightarrow {}^1D_2$, $^3H_6 \rightarrow {}^1G_4$, $^3H_6 \rightarrow {}^3F_3$, and $^3H_6 \rightarrow {}^3H_4$ absorption transitions of the Tm^{3+} ion.[7,18] In Fig. 3, B, C, and E are the excitation spectrum signals of (B) $(Y_{0.995}Tm_{0.005})_3Al_5O_{12}$, (C) $(Y_{0.900}Tm_{0.100})_3Al_5O_{12}$, and (E) $(Y_{0.700}Tm_{0.300})_3Al_5O_{12}$ powder phosphors, respectively.

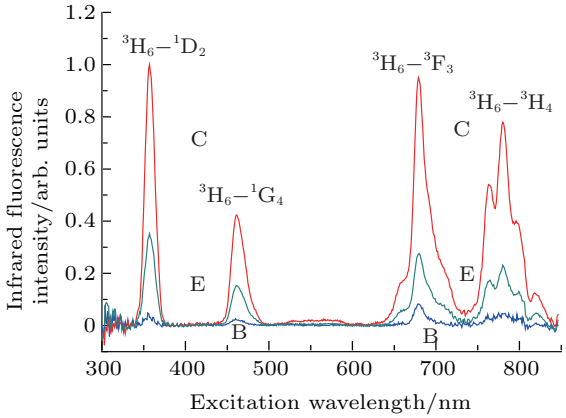


Fig. 3. (color online) Excitation spectra of (B) $(Y_{0.995}Tm_{0.005})_3Al_5O_{12}$ (blue), (C) $(Y_{0.900}Tm_{0.100})_3Al_5O_{12}$ (red), and (E) $(Y_{0.700}Tm_{0.300})_3Al_5O_{12}$ (green) powder phosphors, when the fluorescence received wavelength is located at 1788.0-nm near-infrared wavelength.

5. Experimental luminescence spectra

First, the visible luminescence spectra of the (B) $(Y_{0.995}Tm_{0.005})_3Al_5O_{12}$, (C) $(Y_{0.900}Tm_{0.100})_3Al_5O_{12}$, and (E) $(Y_{0.700}Tm_{0.300})_3Al_5O_{12}$ powder phosphors are measured. The 357.0-nm $^3H_6 \rightarrow {}^1D_2$ excitation peak of the Tm:YAG powder phosphor is selected as the excitation wavelength to measure the luminescence spectra of 418 nm–700 nm and 700 nm–1000 nm as shown in Fig. 4. It is found that a strong luminescence peak is located at (454.0 nm, 460.0 nm), a small peak at (485.0 nm, 493.5 nm), a small peak at (660.5 nm, 669.5 nm), and a medium-sized peak at (785.0 nm, 801.0 nm) for the Tm:YAG powder phosphor. It is easy to recognize that these are respectively due to the luminescence transitions of $^1D_2 \rightarrow {}^3F_4$, $^1G_4 \rightarrow {}^3H_6$, $^1G_4 \rightarrow {}^3F_4$, and $^3H_4 \rightarrow {}^3H_6$.[7,18] In the figure, B is the luminescence spectrum signal of the (B) $(Y_{0.995}Tm_{0.005})_3Al_5O_{12}$ powder phosphor; C*2.5 is that of (C) $(Y_{0.900}Tm_{0.100})_3Al_5O_{12}$ powder phosphor, which is magnified 2.5 times; and E*25 (or E*10) is that of (E) $(Y_{0.700}Tm_{0.300})_3Al_5O_{12}$, which is magnified 25 (or 10) times.

The 680.0-nm $^3H_6 \rightarrow {}^3F_3$ excitation peak of the Tm:YAG powder phosphor is selected as the excitation wavelength to measure the luminescence spectra of 750 nm–1000 nm as shown in Fig. 5. It is found that a medium-sized luminescence peak is located at (784.5 nm, 804.0 nm) of $^3H_4 \rightarrow {}^3H_6$ fluorescence for the Tm:YAG powder phosphor. In Fig. 5, B is the luminescence spectrum signal of (B) $(Y_{0.995}Tm_{0.005})_3Al_5O_{12}$ powder phosphor; C*10 is that of (C) $(Y_{0.900}Tm_{0.100})_3Al_5O_{12}$ powder phosphor, which is magnified 10 times; and E*100 is that of (E) $(Y_{0.700}Tm_{0.300})_3Al_5O_{12}$, which is magnified 100 times.

Then, the infrared luminescence spectra of the (B) $(Y_{0.995}Tm_{0.005})_3Al_5O_{12}$, (C) $(Y_{0.900}Tm_{0.100})_3Al_5O_{12}$, and (E) $(Y_{0.700}Tm_{0.300})_3Al_5O_{12}$ powder phosphors are measured. In the same manner, the 357.0-nm $^3H_6 \rightarrow {}^1D_2$ excitation peak of the Tm:YAG powder phosphor is also selected

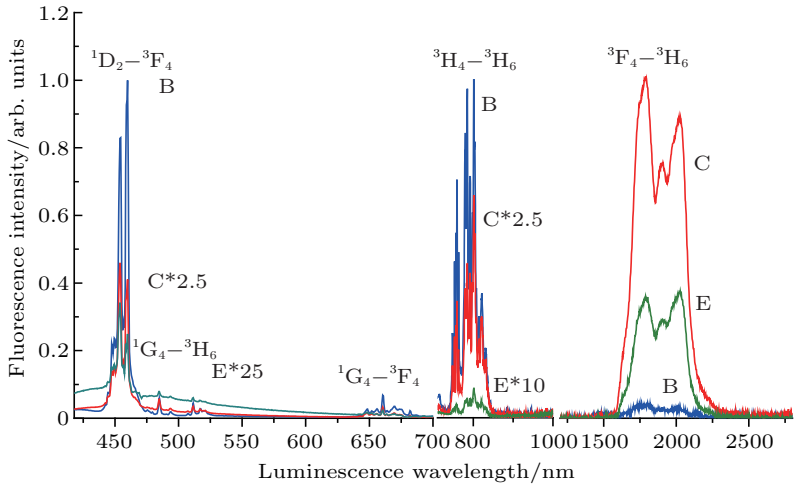


Fig. 4. (color online) Luminescence spectra of (B) $(Y_{0.995}Tm_{0.005})_3Al_5O_{12}$ (blue), (C) $(Y_{0.900}Tm_{0.100})_3Al_5O_{12}$ (red), and (E) $(Y_{0.700}Tm_{0.300})_3Al_5O_{12}$ (green) powder phosphors, when the 357.0-nm $^3H_6 \rightarrow {}^1D_2$ excitation peak is selected as the excitation wavelength.

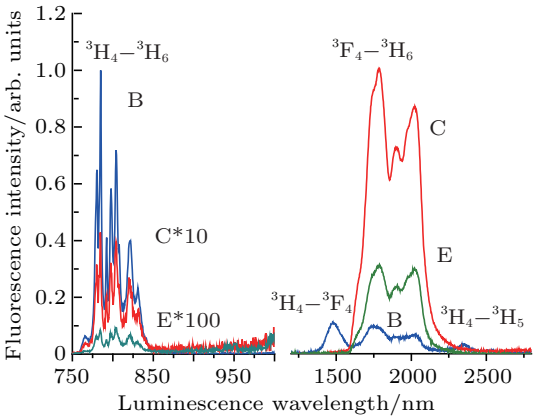


Fig. 5. (color online) The luminescence spectra of (B) $(Y_{0.995}Tm_{0.005})_3Al_5O_{12}$ (blue), (C) $(Y_{0.900}Tm_{0.100})_3Al_5O_{12}$ (red), and (E) $(Y_{0.700}Tm_{0.300})_3Al_5O_{12}$ (green) powder phosphors, when the 680.0-nm $^3H_6 \rightarrow ^3F_3$ excitation peak is selected as the excitation wavelength.

as the excitation wavelength to measure the infrared luminescence spectra of 1200 nm–2800 nm as shown in Fig. 4. It is found that there is a group of strong (1788.0 nm, 1900.0 nm, 2020.0 nm) luminescence peaks for the (C) $(Y_{0.900}Tm_{0.100})_3Al_5O_{12}$ powder phosphor. It is easy to recognize that it is due to the $^3F_4 \rightarrow ^3H_6$ luminescence transition.[7,18] In the figure, B, C, and E are the luminescence spectrum signals of (B) $(Y_{0.995}Tm_{0.005})_3Al_5O_{12}$, (C) $(Y_{0.900}Tm_{0.100})_3Al_5O_{12}$, and (E) $(Y_{0.700}Tm_{0.300})_3Al_5O_{12}$ powder phosphors respectively. It is entirely achieved that the signal intensity is reversed. The near-infrared luminescence signal intensity of the (C) $(Y_{0.900}Tm_{0.100})_3Al_5O_{12}$ and (E) $(Y_{0.700}Tm_{0.300})_3Al_5O_{12}$ powder phosphors is much larger than that of (B) $(Y_{0.995}Tm_{0.005})_3Al_5O_{12}$.

The 680.0-nm $^3H_6 \rightarrow ^3F_3$ excitation peak of the Tm:YAG powder phosphor is also selected as the excitation wavelength to measure the luminescence spectra of 1200 nm–2800 nm as shown in Fig. 5. It is found that the (B) $(Y_{0.995}Tm_{0.005})_3Al_5O_{12}$ powder phosphor has three groups of small luminescence peaks located at 1478.0 nm, (1750.0 nm, 2022.0 nm), and 2352.0 nm. It is easy to recognize that these are respectively due to the $^3H_4 \rightarrow ^3F_4$, $^3F_4 \rightarrow ^3H_6$, and $^3H_4 \rightarrow ^3H_5$ luminescence transitions.[7,18] Meanwhile, it is found that the (C) $(Y_{0.900}Tm_{0.100})_3Al_5O_{12}$ and (E) $(Y_{0.700}Tm_{0.300})_3Al_5O_{12}$ powder phosphors each have only one group of strong $^3F_4 \rightarrow ^3H_6$ luminescence peaks located at 1788.0, 1902.0, and 2020.0 nm respectively.

6. Experimental fluorescence lifetime measurement results

The fluorescence lifetime values of the 460.0-nm and 800.0-nm visible fluorescences of the (A) $(Y_{0.9975}Tm_{0.0025})_3Al_5O_{12}$, (B) $(Y_{0.995}Tm_{0.005})_3Al_5O_{12}$, (C) $(Y_{0.900}Tm_{0.100})_3Al_5O_{12}$, (D) $(Y_{0.800}Tm_{0.200})_3Al_5O_{12}$, and (E) $(Y_{0.700}Tm_{0.300})_3Al_5O_{12}$ powder phosphors, are measured by the Fluorescence Spectrometer FL3-2iHR, produced by the Horiba-JY Company, and shown in Fig. 6 are those of (B) and (C). In the measurements, the pumping sources are the 360-nm NanoLED semiconductor quasi-laser and pulse Xe lamp. All fluorescence lifetime values of 460.0-nm and 800.0-nm fluorescences are fit to the measured fluorescence lifetime curves.[2,5–12] The fitting method is tail fit. The original point is set after equipment response. It is found from the measurements that the fluorescence lifetime values of 460.0 nm and 800.0 nm of (A) $(Y_{0.9975}Tm_{0.0025})_3Al_5O_{12}$ are τ_A(460 nm) = 29.18 μs and τ_A(800 nm) = 479.3 μs, respectively; those of (B) $(Y_{0.995}Tm_{0.005})_3Al_5O_{12}$ are τ_B(460 nm) = 28.32 μs and τ_B(800 nm) = 459.8 μs; those of (C) $(Y_{0.900}Tm_{0.100})_3Al_5O_{12}$ are τ_C(460 nm) = 11.37 μs and τ_C(800 nm) = 138.5 μs; those of (D) $(Y_{0.800}Tm_{0.200})_3Al_5O_{12}$ are τ_D(460 nm) = 10.97 μs and τ_D(800 nm) = 115.2 μs; and those of (E) $(Y_{0.700}Tm_{0.300})_3Al_5O_{12}$ are τ_E(460 nm) = 9.315 μs and τ_E(800 nm) = 96.86 μs.

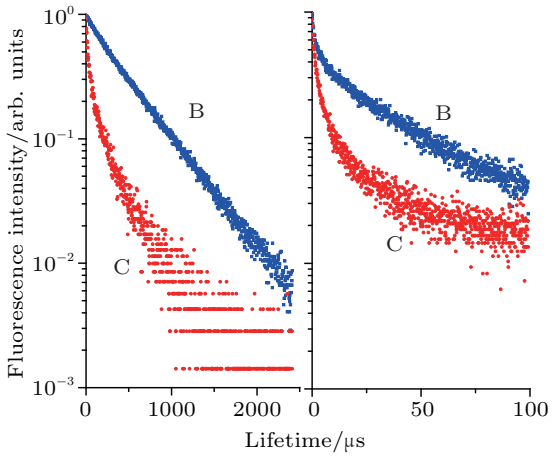


Fig. 6. (color online) Variations of fluorescence intensity with fluorescence lifetime of the 460.0 nm (right) and 800.0 nm (left) visible fluorescence of (B) $(Y_{0.995}Tm_{0.005})_3Al_5O_{12}$ (blue) and (C) $(Y_{0.900}Tm_{0.100})_3Al_5O_{12}$ (red) powder phosphors, when excited by 368.0-nm (right) and 680.0-nm (left) pulsed light respectively.

According to the literature about well-known infrared quantum cutting, the energy transfer efficiency of the Tm^{3+} ion caused by cross-relaxation energy transfer is determined by the following formula:[2,5–12]

$$\eta_{\mathrm{tr},x\%\mathrm{Tm}} \approx 1 - \frac{\int I_{x\%\mathrm{Tm}}\,\mathrm{d}t}{\int I_{0.25\%\mathrm{Tm}}\,\mathrm{d}t}, \tag{1}$$

where I denotes the intensity, and x%Tm represents the Tm^{3+} concentration. In formula (1), it is assumed that the energy transfer among the Tm^{3+} ions is very small when $x = 0.25\%$, which can represent the case of non-energy transfer.

Therefore it can be calculated that the theoretical energy transfer efficiencies of the 460.0-nm and 800.0-nm fluorescences are $\eta_{\mathrm{tr},0.5\%\mathrm{Tm}}$ (460 nm) = 2.947% and $\eta_{\mathrm{tr},0.5\%\mathrm{Tm}}$

(800 nm) = 4.068%, $\eta_{tr,10\%Tm}$ (460 nm) = 61.03% and $\eta_{tr,10\%Tm}$ (800 nm) = 71.10%, $\eta_{tr,20\%Tm}$ (460 nm) = 62.41% and $\eta_{tr,20\%Tm}$ (800 nm) = 75.96%, and $\eta_{tr,30\%Tm}$ (460 nm) = 68.08% and $\eta_{tr,30\%Tm}$ (800 nm) = 79.79%.

7. Analysis

From the above experimental data, the concentration effect of near-infrared quantum cutting luminescence phenomena of $(Y_{1-x}Tm_x)_3Al_5O_{12}$ powder phosphor can be analyzed. The variations of the normalized lifetime of 460-nm fluorescence and the normalized luminescence intensities of 1788-, 785-, 460-nm fluorescence with concentration of Tm^{3+} ion, when excited by 357-nm light, are shown in the left of Fig. 7 by curves *A* (yellow), *B* (red), *C* (blue), and *D* (green) respectively. In the same manner, the variations of the normalized lifetime of 800-nm fluorescence and the normalized luminescence intensities of 1788-, 785-nm fluorescence with concentration of Tm^{3+} ion, when excited by 680-nm light, are shown in the right of Fig. 7 by curves *A* (yellow), *B* (red), and *C* (blue). It is clear that the lifetime decreases monotonically with the increase of concentration, which means that the energy transfer increases monotonically with the increase of concentration. It is obvious that the 1788-nm near-infrared fluorescence intensity first increases and then decreases due to the concentration quenching. It can also be seen that the visible fluorescence intensity decreases very fast with the increase of concentration when the concentration is larger than 0.5%, which means that the concentration quenching in the powder is large.

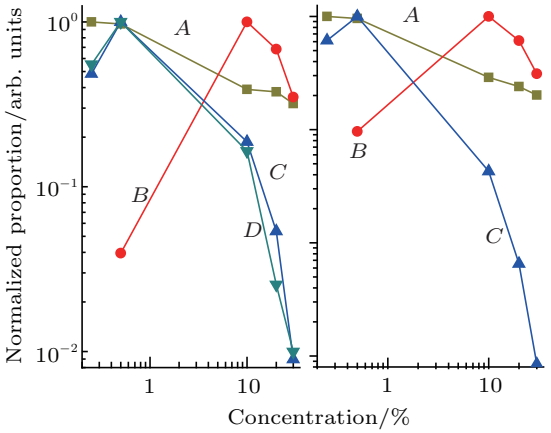


Fig. 7. (color online) Variations of the normalized fluorescence lifetime (yellow) of 460-nm (left) and 800-nm (right) fluorescence and the normalized luminescence intensity of 1788-nm (red), 785-nm (blue), 460-nm (green) fluorescences with concentration of Tm^{3+} ion, when excited by 357-nm (left) and 680-nm (right) light.

The schematic diagrams of energy level structure and quantum cutting process of the $(Y_{1-x}Tm_x)_3Al_5O_{12}$ powder phosphor are shown in Fig. 8.

The main quantum-cutting downconversion process originating from the $^3H_4$ energy level is as follows.[23]

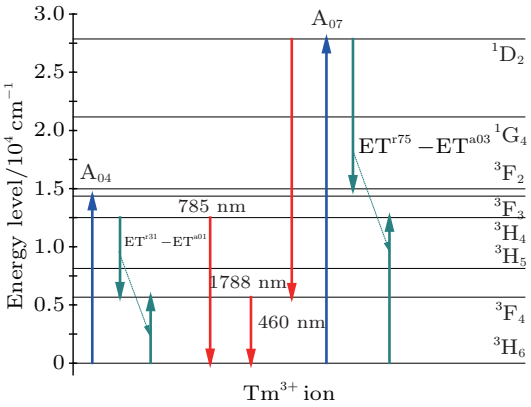


Fig. 8. (color online) Schematic diagram of energy level structure and quantum cutting process of $(Y_{1-x}Tm_x)_3Al_5O_{12}$ powder phosphor.

When the $^3H_4$, $^3F_3$, and $^3F_2$ energy levels are excited, many Tm^{3+} ions may be populated at the $^3H_4$ energy level, because of the rapid multiphonon non-radiative relaxation from the $^3F_3$ and $^3F_2$ energy levels to $^3H_4$. It can be found that Tm^{3+} ion possesses a very effective $\{^3H_4 \rightarrow {}^3F_4,\ ^3H_6 \rightarrow {}^3F_4\}$ CR1: ET^{r31}–ET^{a01} cross-energy transfer process. Although its actual transition mismatch +614.0 cm^{-1} is large, its reduced matrix elements U^2 (0.1275,0.1311,0.2113) and (0.5375,0.7261,0.2382) of Tm^{3+} ion are extremely large,[7,18] therefore the cross-energy transfer rate of $\{^3H_4 \rightarrow {}^3F_4,\ ^3H_6 \rightarrow {}^3F_4\}$ CR1: ET^{r31}–ET^{a01} is also very large. For high-concentration Tm^{3+}-doped YAG powder phosphor, the population of $^3H_4$ energy level may directly transfer to the first excited state $^3F_4$ energy level mainly through the $\{^3H_4 \rightarrow {}^3F_4,\ ^3H_6 \rightarrow {}^3F_4\}$ CR1: ET^{r31}–ET^{a01} cross-energy transfer process. It results in the very effective two-photon near-infrared quantum cutting of the $^3F_4 \rightarrow {}^3H_6$ fluorescence.

Therefore the two-photon near-infrared quantum cutting efficiency of 1788.0-nm $^3F_4 \rightarrow {}^3H_6$ fluorescence, when the $^3F_3$ energy level is excited by 680.0-nm light, can be expressed as follows:

$$\eta_{CR,x\%Tm}(^3H_4) = \eta_{^3H_4} \cdot [1 - \eta_{tr,x\%Tm}(^3H_4)] + 2\eta_{^3F_4}\eta_{tr,x\%Tm}(^3H_4), \quad (2)$$

where $\eta_{CR,x\%Tm}(^3H_4)$ is the two-photon near-infrared quantum cutting efficiency, $\eta_{tr,x\%Tm}(^3H_4)$ is the energy transfer efficiency of the CR1: ET^{r31}–ET^{a01} cross-energy transfer, and $\eta_{^3H_4}$ and $\eta_{^3F_4}$ are the luminescent efficiencies of the $^3H_4$ and $^3F_4$ energy levels of Tm^{3+} ion respectively. We assume that $\eta_{^3H_4} = \eta_{^3F_4} = 1$, as assumed in most of papers about near-infrared quantum cutting.[2,5–12] Therefore, the up-limit of the two-photon near-infrared quantum cutting efficiency of Tm^{3+} ion induced by the CR1: ET^{r31}–ET^{a01} $\{^3H_4 \rightarrow {}^3F_4,\ ^3H_6 \rightarrow {}^3F_4\}$ cross-energy transfer can be expressed as follows:

$$\eta_{CR,x\%Tm}(^3H_4) = 1 + \eta_{tr,x\%Tm}(^3H_4). \quad (3)$$

By calculation it is easy to obtain that

$\eta_{CR,0.5\%Tm}(^3H_4) = \eta_{CR,0.5\%Tm}$ (680 nm) = 104.07%,
$\eta_{CR,10\%Tm}(^3H_4) = \eta_{CR,10\%Tm}$ (680 nm) = 171.10%,
$\eta_{CR,20\%Tm}(^3H_4) = \eta_{CR,20\%Tm}$ (680 nm) = 175.96%,
and
$\eta_{CR,30\%Tm}(^3H_4) = \eta_{CR,30\%Tm}$ (680 nm) = 179.79%.

The main quantum-cutting downconversion processes originating from $^1D_2$ energy level are as follows.[23]

When the $^1D_2$ energy level is excited, many Tm^{3+} ions may be populated at the $^1D_2$ energy level because the $^1D_2$ energy level is a metastable energy state. It can be found that the Tm^{3+} ion possesses a very effective $\{^1D_2 \rightarrow {}^3F_2, {}^3H_6 \rightarrow {}^3H_4\}$ CR10: ET^{r75}–ET^{a03} cross-energy transfer process. Its actual transition mismatch -79.8 cm^{-1} is small, and the reduced matrix elements U^2 (0.0643,0.3065,0) and (0.2357,0.1081,0.5916) of the Tm^{3+} ion are very large,[7,18] therefore the cross-energy transfer rate of $\{^1D_2 \rightarrow {}^3F_2, {}^3H_6 \rightarrow {}^3H_4\}$ CR10: ET^{r75}–ET^{a03} is very large. It is also found that other cross-energy transfer processes have small transfer rates compared with $\{^1D_2 \rightarrow {}^3F_2, {}^3H_6 \rightarrow {}^3H_4\}$ CR10: ET^{r75}–ET^{a03}.

In conclusion, for high-concentration Tm^{3+}-doped YAG powder phosphor, the population of the $^1D_2$ energy level may directly transfer to the lower energy level mainly through the $\{^1D_2 \rightarrow {}^3F_2, {}^3H_6 \rightarrow {}^3H_4\}$ CR10: ET^{r75}–ET^{a03} cross-energy transfer process, i.e., one population of the $^1D_2$ energy level may very effectively lead to two populations of the $^3H_4$ energy level mainly through the $\{^1D_2 \rightarrow {}^3F_2, {}^3H_6 \rightarrow {}^3H_4\}$ CR10: ET^{r75}–ET^{a03} cross-energy transfer process. Consequently it may also very effectively lead to four populations of the $^3F_4$ energy level through the CR1: ET^{r31}–$ET^{a01}\{^3H_4 \rightarrow {}^3F_4, {}^3H_6 \rightarrow {}^3F_4\}$ cross-energy transfer process. It results in the effective four-photon near-infrared quantum cutting of the $^3F_4 \rightarrow {}^3H_6$ fluorescence of Tm^{3+} ion.

The relative proportions of 357.0-nm peak to 680.0-nm peak for the 1788.0-nm excitation spectrum and absorption spectrum of (E) $(Y_{0.700}Tm_{0.300})_3Al_5O_{12}$ powder phosphor, from Figs. 3 and 1, can be easily calculated to be 1.2768 and 0.2913. It is clear that the multi-photon quantum cutting of 1788.0-nm luminescence, when excited by 357.0-nm light, has very large quantum cutting efficiency.

Therefore the four-photon near-infrared quantum cutting efficiencies of the 1788.0-nm $^3F_4 \rightarrow {}^3H_6$ fluorescence, when the $^1D_2$ energy level is excited by 357.0-nm light, can be expressed as follows:

$$\begin{aligned}\eta_{CR,x\%Tm}(^1D_2) = {} & \{\eta_{^1D_2} \cdot [1 - \eta_{tr,x\%Tm}(^1D_2)] \\ & + 2\eta_{^3H_4}\eta_{tr,x\%Tm}(^1D_2)\} \\ & \times \{\eta_{^3H_4} \cdot [1 - \eta_{tr,x\%Tm}(^3H_4)] \\ & + 2\eta_{^3F_4}\eta_{tr,x\%Tm}(^3H_4)\}, \end{aligned} \quad (4)$$

where $\eta_{CR,x\%Tm}(^1D_2)$ is the four-photon near-infrared quantum cutting efficiency, $\eta_{tr,x\%Tm}(^1D_2)$ is the energy transfer efficiency of the CR10: ET^{r75}–ET^{a03} cross-energy transfer, and $\eta_{^1D_2}$, $\eta_{^3H_4}$ and $\eta_{^3F_4}$ are the luminescent efficiencies of the $^1D_2$, $^3H_4$, and $^3F_4$ energy levels of Tm^{3+} ion respectively. We assume that $\eta_{^1D_2} = \eta_{^3H_4} = \eta_{^3F_4} = 1$, as assumed in most of papers about near-infrared quantum cutting.[2,5–12] Therefore, the up-limit of the four-photon near-infrared quantum cutting efficiency of the Tm^{3+} ion induced by both the CR10: ET^{r75}–ET^{a03} $\{^1D_2 \rightarrow {}^3F_2, {}^3H_6 \rightarrow {}^3H_4\}$ and CR1: ET^{r31}–ET^{a01} $\{^3H_4 \rightarrow {}^3F_4, {}^3H_6 \rightarrow {}^3F_4\}$ cross-energy transfers can be expressed as follows:

$$\begin{aligned}\eta_{CR,x\%Tm}(^1D_2) = {} & [1 + \eta_{tr,x\%Tm}(^1D_2)] \\ & \times [1 + \eta_{tr,x\%Tm}(^3H_4)]. \end{aligned} \quad (5)$$

By calculation it is then easy to obtain that
$\eta_{CR,0.5\%Tm}(^1D_2) = \eta_{CR,0.5\%Tm}$ (357 nm) = 107.13%,
$\eta_{CR,10\%Tm}(^1D_2) = \eta_{CR,10\%Tm}$ (357 nm) = 275.52%,
$\eta_{CR,20\%Tm}(^1D_2) = \eta_{CR,20\%Tm}$ (357 nm) = 285.78%,
and
$\eta_{CR,30\%Tm}(^1D_2) = \eta_{CR,30\%Tm}$ (357 nm) = 302.19%.

8. Conclusion

In the present paper, it is found that the (C) $(Y_{0.900}Tm_{0.100})_3Al_5O_{12}$, (D) $(Y_{0.800}Tm_{0.200})_3Al_5O_{12}$, and (E) $(Y_{0.700}Tm_{0.300})_3Al_5O_{12}$ powder phosphors possess intense two-photon quantum cutting luminescence resulting from the CR1: ET^{r31}–$ET^{a01}\{^3H_4 \rightarrow {}^3F_4, {}^3H_6 \rightarrow {}^3F_4\}$ cross-energy transfer. It is found that their up-limits of the two-photon near-infrared quantum cutting efficiencies are approximately 171.10%, 175.96%, and 179.79% respectively. Moreover, it is found that the (C) $(Y_{0.900}Tm_{0.100})_3Al_5O_{12}$, (D) $(Y_{0.800}Tm_{0.200})_3Al_5O_{12}$, and (E) $(Y_{0.700}Tm_{0.300})_3Al_5O_{12}$ powder phosphors have strong four-photon near-infrared quantum cutting luminescences of 1788.0-nm $^3F_4 \rightarrow {}^3H_6$ fluorescence of Tm^{3+} ion, which results mainly from both the CR10: ET^{r75}–$ET^{a03}\{^1D_2 \rightarrow {}^3F_2, {}^3H_6 \rightarrow {}^3H_4\}$ and CR1: ET^{r31}–$ET^{a01}\{^3H_4 \rightarrow {}^3F_4, {}^3H_6 \rightarrow {}^3F_4\}$ cross-energy transfers. Finally, it is also found that the up-limits of the four-photon near-infrared quantum cutting efficiencies are approximately 275.52%, 285.78%, and 302.19% for (C) $(Y_{0.900}Tm_{0.100})_3Al_5O_{12}$, (D) $(Y_{0.800}Tm_{0.200})_3Al_5O_{12}$, and (E) $(Y_{0.700}Tm_{0.300})_3Al_5O_{12}$ powder phosphors respectively. To the knowledge of the authors, it is the first time that a near-infrared quantum cutting efficiency up-limit exceeding 300% has been reported.

Trupke and Green have theoretically derived that the largest energy efficiency limit of the downconversion quantum cutting solar cell is approximately 40%,[22] which is larger than the Shockley–Queisser limit 30%.[15,22] It is important to note that the work of Trupke and Green is based on two-photon quantum cutting, of which the largest quantum cutting

efficiency is close to 200%. However, for four-photon quantum cutting, the largest quantum cutting efficiency may approach 400%. Therefore, it is entirely possible for the largest energy efficiency limit of the quantum cutting solar cell to exceed 40%, thus reaching a higher value for four-photon quantum cutting solar cell. It is valuable for helping to probe the new generation solar cell that was proposed by Green.[20]

Acknowledgment

The authors thank Prof. Liang Jing-Kui, Prof. Zhou Yong-Fen, Prof. Chen Luan, Dr. Ye Yu, Prof. Nie Yu-Xin, Prof. Wang Nai-Yan, Prof. Zhang Zhi-Ying, Prof. Xiao Nan, Prof. Gao Shang-Yu, Prof. Dong Qi, Prof. Feng Bao-Hua, and Prof. Peng Fang-Lin very much for their help.

References

[1] Yang G Z 1995 *Optical Physics* (Beijing: Science Press) (in Chinese)
[2] Vergeer P, Vlugt T J H, Kox M H F, den Hertog M I, van der Eerden J P J M and Meijerink A 2005 *Phys. Rev. B* **71** 014119
[3] Richards B S 2006 *Sol. Energy Mater. Sol. Cells* **90** 1189
[4] Bitnar B 2003 *Semicond. Sci. Technol.* **18** S221
[5] Huang X Y, Han S Y, Huang W and Liu X G 2013 *Chem. Soc. Rev.* **42** 173
[6] Chen D Q, Wang Y S, Yu Y L, Huang P and Weng F Y 2008 *Opt. Lett.* **33** 1884
[7] Reisfeld R 1977 *Lasers and Excited States of Rare-Earth* (Berlin Heidelberg: Springer-Verlag)
[8] Chen X B, Salamo G J, Yang G J, Li Y L, Ding X L, Gao Y, Liu Q L and Guo J H 2013 *Opt. Express* **21** A829
[9] van der Ende B M, Aarts L and Meijerink A 2009 *Adv. Mater.* **21** 3073
[10] Eliseeva S V and Bunzli J C G 2010 *Chem. Soc. Rev.* **39** 189
[11] Sun J Y, Sun Y N and Zhu J C 2013 *Chin. Phys. B* **22** 057803
[12] Zhou J J, Teng Y, Liu X F, Ye S, Xu X Q, Ma Z J and Qiu J R 2010 *Opt. Express* **18** 21663
[13] Shu G W, Lin J Y, Jian H T, Shen J L, Wang S C, Chou C L, Chou W C, Wu C H, Chiu C H and Kuo H C 2013 *Opt. Express* **21** A123
[14] Yu D C, Ye S, Peng M Y, Zhang Q Y, Wondraczek L 2012 *Appl. Phys. Lett.* **100** 191911
[15] van der Ende B M, Aarts L and Meijerink A 2009 *Phys. Chem. Chem. Phys.* **11** 11081
[16] Chen J X, Qiu J R, Ye S and Wang X 2008 *Chin. Phys. Lett.* **25** 2078
[17] Wang G H, Zhao L, Chen J W, Diao H W, Wang G and Wang W J 2013 *Chin. Phys. B* **22** 068102
[18] Xu G X 1995 *Rare Earth* (Beijing: Metallurgical Industry Press) (in Chinese)
[19] Forster T 1948 *Ann. Phys.* **2** 55
[20] Green M A 2003 *Third Generation Photovoltaics: Advanced Solar Energy Conversion* (Berlin: Springer-Verlag)
[21] Wang S M, Du S F, Lu J, Zhang D X and Feng B H 2007 *Chin. Phys.* **16** 1786
[22] Trupke T, Green M A and Wurfel P 2002 *J. Appl. Phys.* **92** 1668
[23] Chen X B, Kang D G, Li S, Wen L, Yu C L, Hu L L and Zhou J 2011 *Chin. Phys. B* **20** 027801
[24] Dexter D L 1957 *Phys. Rev.* **108** 630
[25] Shen X L, Li Z C, Shen C X, Lu W, Dong X L, Zhou F and Zhao Z X 2009 *Chin. Phys. B* **18** 2893
[26] Lin H, Chen D Q, Yu Y L, Zhang R and Wang Y S 2013 *Appl. Phys. Lett.* **103** 091902
[27] Wang Y Z, Yu D C, Lin H H, Ye S, Peng M Y and Zhang Q Y 2013 *J. Appl. Phys.* **114** 203510
[28] Lin H, Chen D Q, Yu Y L, Yang A P and Wang Y S 2011 *Opt. Lett.* **36** 876
[29] Lin H, Marque′s-Hueso J, Chen D Q, Wang Y S and Richards B S 2012 *Mater. Res. Bull.* **47** 4433
[30] Lin H, Chen D Q, Yu Y L, Shan Z F, Huang P, Yang A P and Wang Y S 2011 *J. Alloys Compd.* **509** 3363